Airflow and Water-Drop Trajectories at Instrument Sampling Points around the Beechcraft King Air and Lockheed Electra

CYNTHIA H. TWOHY AND DIANA ROGERS

National Center for Atmospheric Research, Boulder, Colorado*

(Manuscript received 23 January 1992, in final form 17 November 1992)

ABSTRACT

Due to distortion of airflow streamlines, flow velocities and droplet size distributions measured around a moving aircraft can differ from freestream conditions. This can complicate measurements made from aircraft platforms. Potential flow calculations were used to predict airflow characteristics and the spatial distribution of different-sized droplets around the Lockheed Electra L-188 and Beechcraft King Air-200 aircraft at a variety of instrument mounting locations. Large deviations from freestream conditions were found to occur at certain locations on both aircraft near the fuselage and in regions of strong curvature. The number concentration of droplets 100–200 μm in diameter is most seriously affected by flow distortion effects. Calculation results were in reasonable agreement with measurements at a forward mounting location on the King Air.

1. Introduction

Flow velocity and droplet distributions near a moving aircraft may differ from freestream values. Droplet trajectories may be affected as airflow streamlines are distorted by the passage of the aircraft. In general, very small droplets (less than 10 μm in diameter) and aerosol particles approximately follow flow streamlines, while very large droplets (greater than 500 μm in diameter) tend to maintain their initial direction and speed. Intermediate-sized droplets deviate from their initial trajectories in the direction of, but not along the exact path of, the streamlines. This leads to "shadow zones," areas near the fuselage that are bypassed by trajectories of intermediate-sized droplets, and "enhancement regions," areas outside of the shadow zones where the deflected trajectories converge. Droplet number concentrations are higher in enhancement regions than in the freestream, but are essentially zero in shadow zones.

Particle and hydrometeor measurements from aircraft platforms are complicated by these effects of the airflow around the aircraft. Cloud droplets 100–200 μm in diameter are especially prone to enhancement and shadow zone effects. Aerosol particles are typically less than a few micrometers in diameter and therefore tend to follow flow streamlines. However, aerosols may still be difficult to sample accurately. One reason is that local flow speed at the tip of an aerosol inlet may differ considerably from the aircraft speed. The local flow speed is needed to establish isokinetic sampling requirements and the air volume actually sampled. In addition, the flow direction at the sampling point may vary substantially from the direction of aircraft motion and degrade the collection characteristics of inlets that are not properly aligned.

Because the flow field around an aircraft is not usually known a priori, correct placement and use of sampling instrumentation can be difficult. In this study, theoretical calculations of flow velocity and droplet trajectories were made for different mounting locations and distances from the fuselage of the Beechcraft King Air-200 and Lockheed Electra L-188; these aircraft are operated by the National Center for Atmospheric Research (NCAR). At two mounting locations on the King Air, liquid water content was measured at various distances from the fuselage for comparison with calculations. Our findings should aid in judicious placement and use of droplet-measuring instruments on the aircraft.

2. Previous work

The airflow patterns around specific aircraft have been investigated in several other studies. A few of these studies actually involved measurements, but most utilized potential flow calculations to predict flow characteristics and droplet trajectories. Norment (1976), using the same code that generated the results of this paper, used three-dimensional aircraft models to calculate droplet trajectories around a Cessna Citation and a Lockheed C-130. This study predicted that two droplet sampling instruments mounted on the Citation were located in an enhancement region for droplets

* The National Center for Atmospheric Research is sponsored by the National Science Foundation.

Corresponding author address: Dr. Cynthia H. Twohy, NCAR, P.O. Box 3000, Boulder, CO 80307.

100–200 μm in diameter and that a small change in instrument placement could have a large effect on droplet number concentrations. For 100-μm droplets, the concentration factor, defined as the ratio of droplet flux at the sampling point to droplet flux in the freestream, ranged from about 1.7 for one instrument location to over 5.0 for an instrument mounted slightly higher on the side of the fuselage. It was also predicted that the intake slit of a particle replicator mounted on the side of the C-130 fuselage was located in a shadow zone for droplets 100–300 μm in diameter. At the same mounting location but farther out from the fuselage, these droplet sizes were substantially enhanced in number concentration. At progressively larger distances from the fuselage, however, the enhancement was less severe. This type of behavior has also been predicted by airflow studies at NCAR.

A simpler axisymmetric model was used by King (1984) to calculate flow potential and droplet trajectories around the fuselage of a Fokker F-27. He developed a general description of the flow field (away from the body and regions of high curvature) in terms of the distance behind the nose and the fuselage radius; it was shown that at locations just behind the cockpit, flow speeds could be enhanced by 5%–10% over freestream values. Droplet behavior was also generalized in terms of a nondimensional number, S, similar to the Stokes number.

King et al. (1984) compared model predictions with measurements around the F-27. Flow speed measured with a pitot-static tube and droplet enhancement and shadow zones measured with a hot-wire probe were in general agreement with model-calculated parameters. In a later paper (King 1985), a simple algorithm for the width of the shadow zone as a function of S and distance behind the cockpit was developed; the model was also extended to predict the behavior of irregularly shaped particles.

Particle Measuring Systems (PMS) probes are widely used in aircraft studies to measure optically the size distribution of aerosol particles and droplets. Large variations in flow velocity occurring upstream of the probe canisters (housings) were shown by Beard (1983) and King (1986) to affect the orientation of hydrometeors entering the sampling plane of the instruments. Calculations of flow about wing-mounted PMS probes were used by Drummond and MacPherson (1985) and Norment (1988) to demonstrate that flow velocities at the PMS sampling point could be considerably lower than freestream. The assumption that flow and droplet speeds are equivalent to the aircraft speed could therefore lead to substantial errors, for example, in 2D images produced by a scanning laser or in the sample volume used to calculate droplet concentrations. MacPherson and Baumgardner (1988) used a Rosemount 858 five-hole pressure sensor to measure the flow speed and angle ahead of wingtip-mounted PMS probes on a King Air; they found significant flow distortion due to the wing, pylon, and PMS canisters themselves.

3. Measurements around the Beechcraft King Air

a. Experimental design

The goal of the first part of this study was to measure the variation in liquid water content at different distances from the fuselage of the King Air; the measurements were then compared with droplet trajectory calculations for some of the same locations. Simultaneous measurements of cloud liquid water content were made with two PMS–CSIRO hot-wire probes (King et al. 1978; 1981) mounted on the King Air. These probes operate by measuring the amount of power necessary to maintain their heated sensing element at a constant temperature while the element loses heat due to convection and evaporation of cloud droplets.

Using an approach similar to that of King et al. (1984), the two probes were mounted at the same distance behind the nose of the aircraft and the same distance either side of the aircraft centerline. One was fixed at 43 cm above the aircraft fuselage, while the other was attached to a strut that could be retracted in flight. The latter probe was extended out to 43 cm for takeoff and landing, but was retracted to different distances from the fuselage while flying in both clear and cloudy air. (For structural reasons, 43 cm was the maximum distance that the probe could be extended.) Assuming symmetry about the vertical–longitudinal plane and that differences in the measurements were only due to the distance of the probe from the fuselage, the fixed probe was used as a standard for comparison with the retractable probe at various positions. The majority of measurements were taken close to the fuselage, where variations in liquid water content were expected to be greatest.

The traditional aircraft coordinate system describes position in terms of inches along three axes: "fuselage station" (FS), the longitudinal axis of the aircraft; "butt line" (BL), the horizontal axis perpendicular to the FS axis; and "water level" (WL), a vertical axis perpendicular to the other two. The zero datum plane (zdp), or plane chosen as the zero reference for the FS axis, is approximately 8 cm aft of the front of the radome on the NCAR King Air and 107 cm ahead of the radome on the NCAR Electra. For the WL axis, the zdp is 191 cm below the bottom of the fuselage on the King Air and 208 cm below the fuselage bottom on the Electra. As this coordinate convention is standard in all information from the aircraft manufacturer and in internal communications regarding instrument mounting, it will be used throughout this paper.

Four mounting locations on the King Air were used for the experiment: two just behind the cockpit at FS 155 (3.94 m behind the zdp of the aircraft), and the other two farther aft at FS 263 (6.68 m behind the

zdp). These overhead locations are often used for aerosol and droplet collection devices, and are shown as points A and C in Fig. 1. The two probes at each station were placed symmetrically on the upper surface of the fuselage, with the supporting struts positioned perpendicular to the fuselage surface, and the strut bases at BL −18 and +18 (46 cm to each side of the aircraft centerline). A PMS forward-scattering spectrometer probe (FSSP-100), which measures the size distribution of cloud droplets approximately 2–50 μm in diameter (Knollenberg 1981), was mounted underneath the wing on the left side of the aircraft at BL −281.

Data were taken during two flights in northeastern Colorado in May 1989. Cloud types encountered ranged from very small cumuli to horizontally extensive stratocumulus decks. Speed runs were made in clear air to obtain calibration data for the convective heat losses of both probes.

b. Data analysis

The amount of power lost through droplet evaporation on the hot-wire probe is the difference between the total power expended by the probe and the power lost due to convection. The Appendix describes how the convective heat loss was determined. Once the power loss to the droplets P_W was determined from this difference, the liquid water content W was calculated as follows:

$$W = P_W\{ldV[L_v + c(T_b - T_a)]\}^{-1}.$$

Here, l and d are the sensor length and diameter, V the local flow speed, L_v the latent heat of vaporization, c the specific heat of water, and T_b and T_a the boiling point of water and the air temperature, respectively. The approach described in the Appendix to calculate the convective heat loss may produce a "baseline," or out-of-cloud, value for liquid water content slightly different from zero; the offset, or difference between the baseline value and zero, is typically ±0.02 g m^{-3}. To reset the baseline to zero and maximize agreement between the probes prior to cloud entry, the offset of each probe in clear air was averaged every 3 s and subtracted from the baseline.

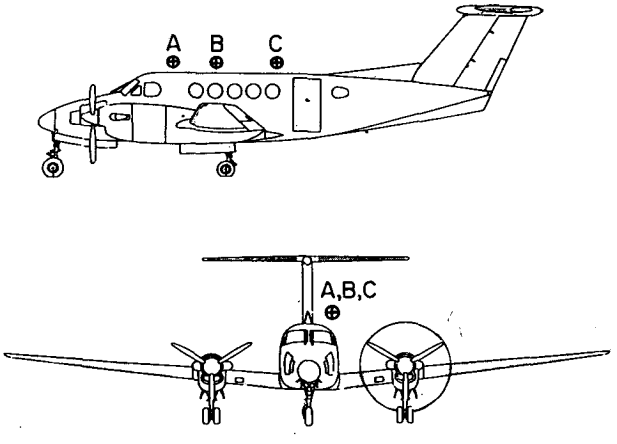

FIG. 1. King Air mounting positions discussed in the text. Positions A and C are the locations of the hot-wire probes used for liquid water measurements. Aircraft coordinates corresponding to these positions are given in Table 1.

The speed of the airflow will change as the streamlines diverge around the aircraft. Therefore, flow speed, as well as liquid water content, was expected to vary at different distances from the fuselage. Liquid water content calculated from the hot-wire probe measurements is inversely proportional to flow speed around the wire; the local flow speed at each distance from the fuselage was therefore needed. To approximate the local flow speed, the probes were used like hot-wire anemometers: as described in the Appendix, the measured power consumption of the probes in clear air was used to calculate the change in flow speed with distance from the fuselage. The resulting speeds may be strongly influenced by temperature and turbulence at the probe location and, in general, do not agree well with model-calculated flow speeds (Appendix). However, the flow speed derived from the probe provided the most reasonable baseline value outside of cloud and was used to calculate liquid water content from the in-cloud probe response.

The uncertainty in liquid water content measured by a hot-wire probe is caused primarily by the offset of the baseline from zero and the imperfect collection efficiency of the probe for very small and very large droplets (D. Baumgardner, personal communication). Losses related to collection efficiency are expected to be approximately equal for both probes, so the main uncertainty in the differences in liquid water content measured by the two probes is expected to result from differences in their baseline values (this difference being approximately ±0.005 g m^{-3}). However, the liquid water values measured by the retractable probe at 43 cm from the fuselage were, on average, 0.006 g m^{-3} lower than the reference probe value at FS 155 and about 0.012 g m^{-3} higher than the reference (fixed probe) value at FS 263. Liquid water values from the two probes were included in our analysis only when the average reference liquid water content was at least 0.10 g m^{-3}, in order to minimize the effect of these uncertainties on the comparison. An additional source of uncertainty arose from the flow speed derived from the hot-wire probe, which was then used to calculate liquid water content. The magnitude and sign of this uncertainty varied with position, but in most cases, was less than 0.002 g m^{-3}. These three sources of uncertainty were added for a few representative points and are depicted with error bars in Figs. 2 and 3.

c. Results

The percent change in liquid water content at various distances from the fuselage at FS 155 relative to that

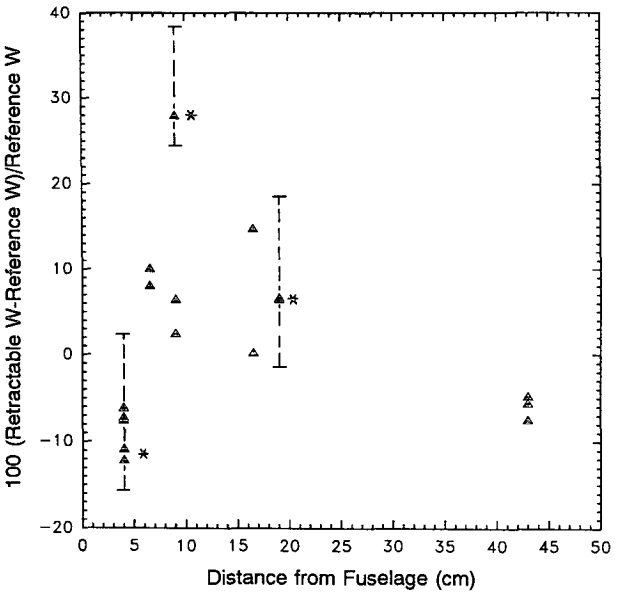

FIG. 2. Percent difference between liquid water content measured at King Air position *A* (FS 155) at different distances from fuselage and that measured at 43 cm from fuselage. Starred points are those for which error bars are shown.

measured by the fixed probe at 43 cm is shown in Fig. 2. The figure shows that liquid water content is depleted at 4 cm from the fuselage at FS 155, but is actually slightly enhanced at distances between 6 and 19 cm out. This mounting location is directly behind the aircraft windscreen, a region of high curvature where droplets with sufficient inertia will deviate from flow streamlines. Mass-weighted mean droplet diameters calculated from the FSSP data were between 10 and 15 μm, droplet sizes that would not be expected to deviate substantially from streamlines. However, as discussed subsequently, calculations indicate that droplets at least as small as 20 μm may exhibit nontrivial inertial effects.

The liquid water profile measured at FS 263 (2.74 m behind FS 155) clearly shows a decrease in water content near the fuselage, with almost 70% depletion at a distance of 4 cm (Fig. 3). Both the frictional boundary layer and shadow zones are thicker farther aft; thus, some depletion of cloud-sized droplets is expected near the fuselage at this location. Considerable scatter in the amount of liquid water remaining at each distance from the fuselage is evident. This is also expected since shadow zones are a function of droplet size, and mass-weighted droplet diameters in the sampled clouds ranged from about 9 to 19 μm. At any given distance from the fuselage, a greater depletion of liquid water was observed when clouds with larger mean droplet diameters were sampled. This is consistent with an increase in shadow zone width with increasing droplet size for cloud-sized droplets, as implied by King (1984). However, as discussed below, droplet concentrations at this location may have also been influenced by an obstruction ahead of the sampling point.

d. Effect of flow obstructions

Any protuberance on an aircraft can alter airflow patterns. Competition for mounting locations often occurs during aircraft missions, and it is unusual for a sensor or inlet to be entirely isolated from other external instruments flown simultaneously. The alignment of the mounting locations on each side of the King Air fuselage requires that when any two instruments are mounted on the same side of the aircraft, one must be placed in front of the other. In this experiment, another droplet measuring device, a counterflow virtual impactor (CVI), was mounted about 1.5 m upstream of the retractable hot-wire probe when the retractable probe was located at FS 263. The CVI, which extended 46 cm above the fuselage, presented a cylindrical obstruction 6 cm in diameter to the flow in that region.

One probable consequence of this obstruction is shown in Fig. 4. The top trace is flow speed determined from the fixed probe at 43 cm and the bottom trace is speed determined from the retractable probe at various distances from the fuselage. (Note the difference in the ordinate scales.) There is a periodic variation in flow speed measured by the probe located behind the CVI, with the greatest amplitude occurring between 6 and 14 cm from the fuselage. This fluctuation was not seen in the signal from the probe mounted in the forward location or from the reference probe mounted on the other side of the aircraft.

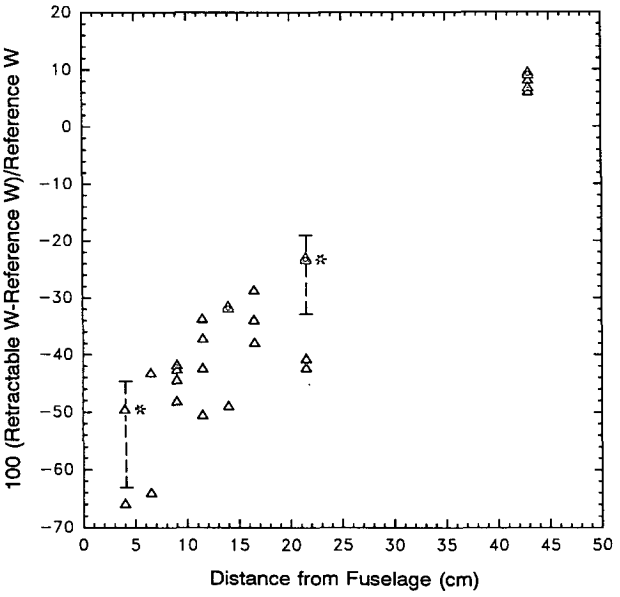

FIG. 3. Percent change between liquid water content measured at King Air position *C* (FS 263) at different distances from fuselage and that measured at 43 cm from fuselage. Starred points are those for which error bars are shown.

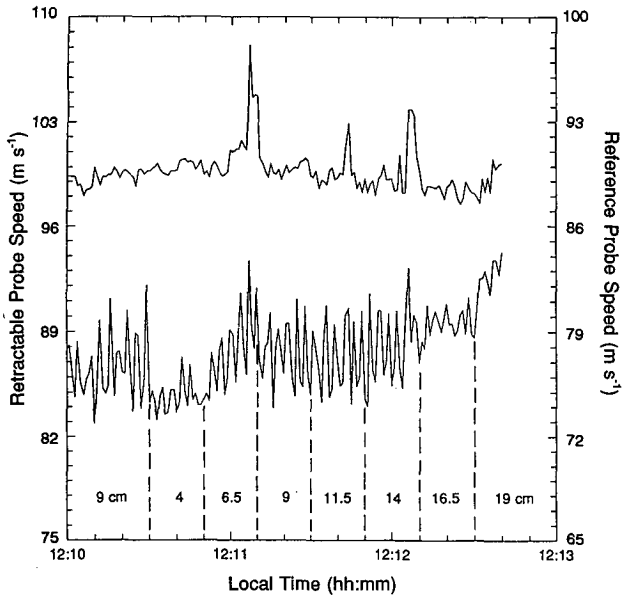

FIG. 4. Time series of flow speed measured by fixed probe at 43 cm (top trace) and retractable probe (bottom trace) at various distances from fuselage at King Air position *C* (FS 263).

Periodic motions of the aircraft itself may have accentuated the flow disturbance: in this case, the apparent changes in flow speed occurred at the same frequency as small variations in the sideslip angle of the aircraft (Fig. 5). A change in sideslip angle could change the relative orientation of the hot-wire and the CVI with respect to the oncoming airspeed vector, moving the hot-wire probe in and out of the wake of the CVI. Although the speed of the airflow would be expected to slow in the wake, it is also possible that turbulence generated by the wake caused an artificial increase in flow speed derived from the hot-wire probe (Appendix). Therefore, it is as yet unclear whether the apparent increases in flow speed correspond to the probe being in or out of the wake. The airflow blockage presented by the CVI may have also contributed to the substantial decrease in liquid water measured by the hot-wire probe near the fuselage at FS 263.

4. Theoretical calculations

a. Aircraft models and code calculations

Two of NCAR's aircraft, the Lockheed Electra L-188 and Beechcraft King Air-200, have been modeled for use with potential flow and trajectory codes in order to predict the flow speed, flow angle, and droplet distributions at various instrument mounting locations and distances from the fuselage. The codes used are those of Norment (1985), which yield a potential flow solution about an arbitrarily shaped body. To use the codes, a paneled model of the aircraft is needed; that is, the actual continuous body is approximated by one composed of contiguous, plane quadrilaterals (e.g., Cooper and Rogers 1991; Fig. 1). The paneled models of the fuselages of the two aircraft were constructed by Hillyer Norment from drawings supplied by the manufacturers; the Electra wing model was constructed subsequently at NCAR. One set of codes calculates potential flow around the modeled body; it allows distributed sources on each of the panels, and calculates the strengths of these sources with the requirement that there be no flow through the panels representing the aircraft shape. Another set of codes uses the potential flow results to calculate trajectories of droplets to user-defined points around the aircraft. The reader is referred to Norment (1985) for details of these calculations. A total of 2098 panels were used to reproduce the King Air, and 1862 were used for the Electra. The higher number of panels for the King Air corresponds to a greater resolution of the aft end of the fuselage.

Several other studies have used potential flow codes successfully. Wyngaard et al. (1985) simulated the flow about a sphere and demonstrated that the numerical solution duplicated the analytical potential flow solution. MacPherson and Baumgardner (1988) showed that the calculated flow ahead of a PMS probe agreed with measurements. Also, the expected offset in pressure at the radome pressure port locations on the NCAR Electra was calculated and found to agree well with the experimentally determined difference.

Because the code calculates potential flow, the solution is not valid within the frictional boundary layer of the aircraft, or under turbulent conditions. In addition, the presence of a thick boundary layer, which would distort the effective shape of the body, is not included in the current analysis. Only the fuselage of the King Air has been modeled at this time, not the wing or propellers, so results are most applicable to

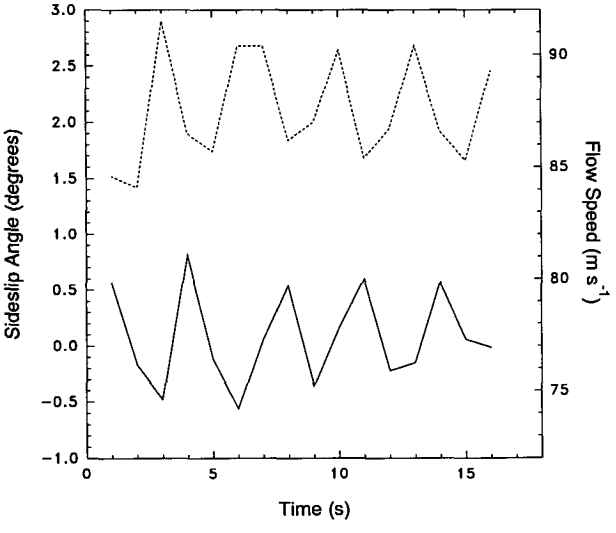

FIG. 5. Aircraft sideslip angle (bottom solid line) and flow speed (top dotted line) derived from the retractable probe when it was located 14 cm from the King Air fuselage at position *C* (FS 263).

regions not strongly affected by these features. The forward mounting locations should be well represented by the model, but the rear locations have a thicker boundary layer, and may also be influenced by the wing and propellers. Results at these locations therefore may be less accurate than at the forward locations. The hot-wire probes that were mounted on the King Air fuselage for the aforementioned measurements have not been included in the model, as both the probes and their mounting struts (6 cm in diameter) were very much smaller than the aircraft fuselage and were assumed to have a relatively small effect on the flow. On the Electra, the PMS probe canisters, which have been shown to have a significant effect on flow characteristics, were also modeled in several cases.

Once the potential flow pattern for a given model configuration is known, the trajectory code calculates the trajectory of a droplet of specified size to any target point near the aircraft. A series of trajectories that lead to a small area at the target plane is calculated; the concentration ratio, or ratio of droplet number concentration at the target to droplet number concentration in the freestream, may then be obtained. Concentration *ratio* is the concentration *factor* discussed earlier divided by the droplet speed (nondimensionalized by freestream speed). Trajectory calculations assume droplets have the density and drag characteristics of water droplets.

The angle of attack was set at two degrees for the King Air and three degrees for the Electra; these are typical attack angles during research flight segments. Atmospheric parameters used in the King Air calculations corresponded to average flight conditions throughout the measurement period (true airspeed of 95 m s^{-1}, ambient temperature of 275 K, and pressure of 720 mb). For the Electra, 125 m s^{-1} and standard conditions of 273 K and 1013 mb were used; the sea level pressure corresponds to conditions in the marine boundary layer where many of the Electra missions are flown. The fuselage diameter used in the calculations was 1.79 m for the King Air and 3.45 m for the Electra. Dimensions of the Electra wing were 15.09 m for the semispan, 2.31 m for the tip chord, and 5.77 m for the root chord.

b. Model results: King Air

1) FLOW CHARACTERISTICS

Flow characteristics and droplet concentration ratios were calculated for the three overhead mounting locations on the King Air shown in Fig. 1. Locations *A* and *C* correspond to the positions of the hot-wire probes that were used to measure liquid water content (FS 155 and 263); location *B* was where the counterflow virtual impactor was mounted (FS 202). Aircraft coordinates for these locations are given in Table 1.

Flow speed and angles were predicted for a range of distances from the aircraft fuselage, from 8 to 43 cm at the forward station and from 13 to 43 cm at the aft station. The smallest distance was chosen in order to avoid the boundary-layer region that would exist on the actual aircraft; the largest distance corresponded to the farthest extension of the hot-wire probes used for the measurements. The results are summarized in Table 1. For a distance 43 cm from the fuselage, the model calculated a 5.3% increase over the freestream airspeed for the forward mounting location and a 2.3% increase over freestream for the rear location. However, the relative speed increase between 43 cm and 13 cm was only 1.1% in the forward location and 0.4% in the rear location. The flow tends to be more parallel to the fuselage and closer to the freestream speed at locations farther back on the fuselage. These results may be useful in inlet design and calculation of air sampling rates.

2) DROPLET TRAJECTORIES

Calculated concentration ratios at the location of the hot-wire probes for selected droplet sizes and distances from the King Air fuselage are shown in Fig. 6 (location *A*) and Fig. 7 (location *C*). Note that the concentration ratios (vertical axes) in these and the

TABLE 1. Model-calculated flow characteristics—King Air.

Location	FS	BL	WL	Y (cm)	$\frac{V_T}{V_\infty}$	α (deg)	β (deg)
A	155.0	25.7	157.2	43	1.053	2.2	0.2
	155.0	20.3	146.5	13	1.064	1.3	0.5
	155.0	19.4	144.7	8	1.065	1.2	0.7
B	202.0	26.2	158.0	48	1.026	1.5	−0.8
	202.0	25.7	157.2	43	1.026	1.5	−0.6
C	263.0	25.7	157.2	43	1.023	1.2	−0.7
	263.0	20.3	146.5	13	1.027	1.4	−1.1

Notes: All calculations are for 2° angle of attack. Locations are as shown in Fig. 1. Here, Y is distance out, normal to fuselage; V_T/V_∞ is ratio of flow speed at target location to freestream speed; α is the vertical flow angle with respect to longitudinal (FS) axis (positive values up); β is the horizontal flow angle with respect to longitudinal (FS) axis (positive values away from fuselage).

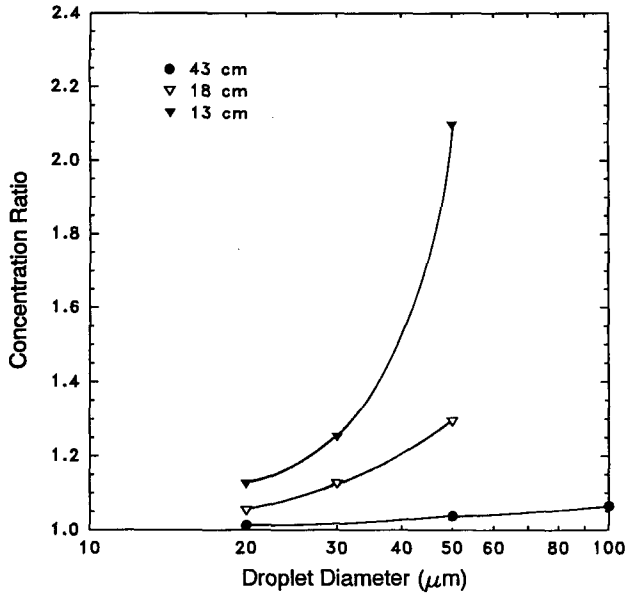

FIG. 6. Calculated concentration ratios for various droplet diameters at 43, 18, and 13 cm from the fuselage for King Air position *A* (FS 155).

other figures in this paper are plotted on different scales in order to depict as much detail of the curve shape as possible. Enhancement effects, as evidenced by higher concentration ratios, are generally more pronounced for locations closer to the fuselage and for droplets near 100 μm in diameter. With increasing proximity to the fuselage, concentration ratios increase systematically until a shadow zone may occur for some droplet sizes. Although not immediately apparent in Fig. 6, a shadow zone was predicted for 100 μm droplets at 18 and 13 cm from the fuselage at location *A*. A shadow zone, if present, is more evident when calculations are extended up to droplet sizes near 1 mm (e.g., Fig. 12).

Calculations for droplets up to 100 μm in diameter at the aft King Air location (Fig. 7) also indicated that concentration ratios increase in magnitude at points closer to the fuselage and for larger droplets. It is interesting to note that at 43 cm, the concentration ratio for 100-μm droplets is 1.17, compared to only 1.10 in the forward position. In fact, the effects of flow distortion extend farther out from the fuselage for all droplet sizes in the aft position. Another point of interest is that in both mounting locations, even droplets as small as 20 μm can experience some enhancement at locations near the fuselage. (Twenty microns is the smallest size considered here, primarily because of computational difficulties for smaller droplets. These difficulties are probably a result of the computer platform used: a Masscomp minicomputer.)

At point *B*, where the CVI inlet was located 46 cm out from the fuselage, concentration ratios were calculated for a full range of droplet sizes (Fig. 8). Concentration factors are also included for comparison; the two quantities differ by a factor equal to the nondimensionalized particle speed. The curve has a maximum at 145 μm in diameter, the size most susceptible to inertial effects. King (1984) generalized droplet behavior in terms of a nondimensional number *S*:

$$S = \frac{2a^2 V_\infty \rho_w}{9\eta b}.$$

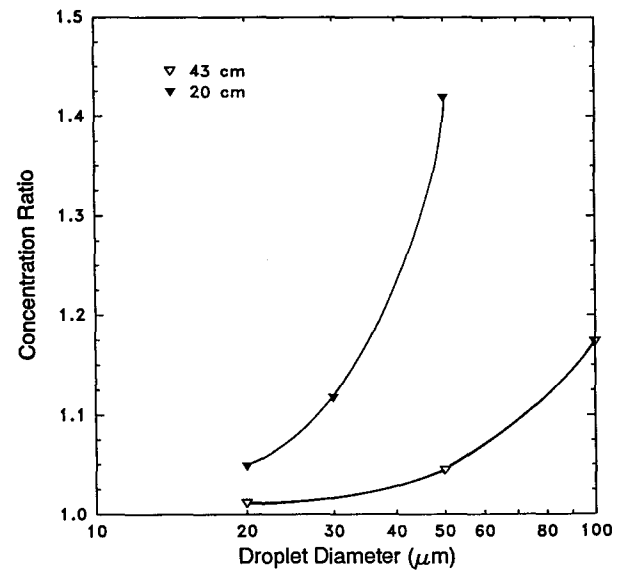

FIG. 7. Calculated concentration ratios for various droplet diameters at 43 and 20 cm from the fuselage for King Air position *C* (FS 263).

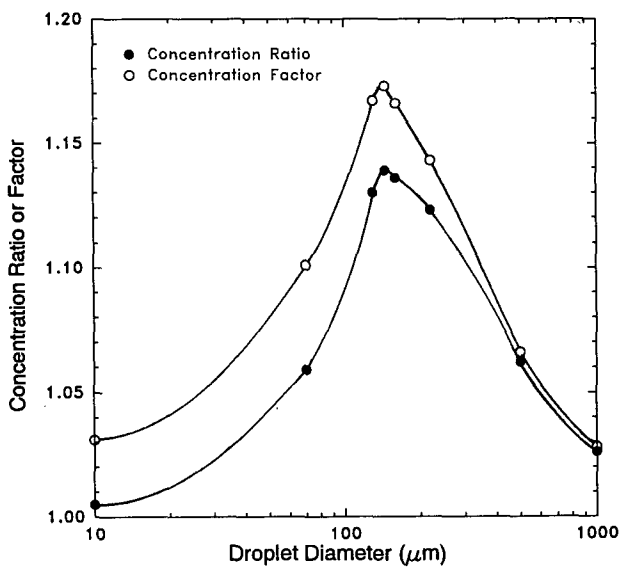

FIG. 8. Calculated concentration ratios and factors as a function of droplet diameter at 46 cm from the fuselage for King Air position *B* (FS 202).

Here, V_∞ is the freestream flow speed, a is the droplet radius, ρ_w is droplet density, η is dynamic air viscosity, and b is the fuselage radius. Along a droplet trajectory, S is constant, while the traditional Stokes number Stk includes $C_d\mathrm{Re}/24$, which varies along the trajectory. The shadow zone width and concentration factors were shown to be at a maximum when S was approximately equal to 6. Using values for the King Air of $a = 72$ μm and $V_\infty = 95$ m s^{-1}, we obtain S equal to 7, in approximate agreement with King's predictions.

c. *Comparison of model and experimental results on King Air*

As discussed in the Appendix, the uncertainty in the flow speeds derived from the hot-wire probe was too large to produce a meaningful comparison with computed flow speeds; therefore, only predicted versus observed droplet behavior is considered here. In the forward location on the King Air, the model-calculated concentration ratio for 20-μm droplets increased about 4% between 43 and 18 cm and about 11% between 43 and 13 cm (Fig. 6). These results are generally consistent with our measurements at this location. Relative to the reference measurement at 43 cm, the average increase in liquid water content was 7% at points 16–19 cm from the fuselage and 11% at points 6–9 cm from the fuselage. The wing-mounted FSSP probe indicated that droplet distributions had mass-weighted mean diameters of 10–15 μm. For a more quantitative comparison, measured droplet distributions from the FSSP and concentration ratios for a variety of small droplet sizes at the actual distances used would be employed to calculate expected liquid water content changes; however, as mentioned before, computational difficulties did not permit this approach.

For the rear location, while the measurements indicated depletion of droplets 20 μm and smaller at less than 20 cm from the fuselage, the model predicted about a 5% enhancement of 20-μm droplets at 20 cm out. Because the model does not include the effects of the frictional boundary layer or the aircraft wing, it may not describe the flow or predict droplet behavior as accurately in the rear location as in the forward one. The aircraft boundary layer will make the fuselage size effectively larger in the rear, which means characteristics predicted to occur at one distance from the fuselage may actually correspond to distances farther from the fuselage. The CVI, mounted directly ahead of the hot-wire probe, is also likely to have changed the flow field and droplet trajectories from those predicted by the model. At this time, the effect of the CVI on droplet trajectories is uncertain, but the periodic oscillation in the retractable probe signal (Figs. 4 and 5) demonstrates that a flow disturbance was present. This may have added to the shadowing effect of the aircraft itself in the rear location.

d. *Model results: Electra*

On the Electra, we have evaluated flow patterns and concentration ratios at several different mounting locations. Figure 9 shows the positions considered, which include overhead and side locations. All these locations are located well ahead of the wing, except the wingtip locations E and F, which are 61 cm above and below the wing, respectively, and 18 cm ahead of the wingtip leading edge. Table 2 lists the aircraft coordinates of the various positions. (Because aircraft coordinates can be somewhat difficult to interpret, the distance away from the aircraft fuselage is also listed in the tables.) Positions A–D are routinely used for aerosol and droplet sampling; these are the positions for which droplet trajectories, in addition to flow characteristics, were calculated.

1) Flow characteristics

The flow speeds and angles predicted by the potential flow code are summarized in Table 2. Because PMS probes are often mounted at positions A and D, the PMS canisters themselves have also been modeled for these locations. The pylons supporting the canisters were not modeled. The actual points considered are where the sampling plane is located, slightly ahead of the canister. Two different configurations have been used for the side location (D), so both were modeled. The primary difference between the two configurations is in distance from the fuselage (28 vs 46 cm). Since this side mounting location is occasionally utilized for other smaller types of samplers, the PMS canister was removed in one simulation. Calculations were also

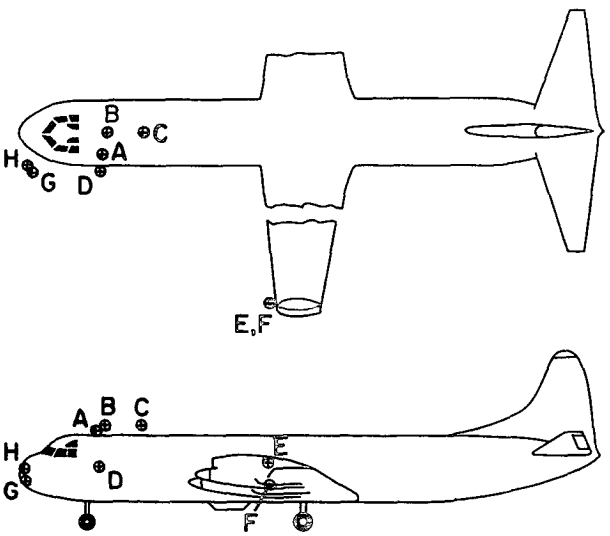

FIG. 9. Electra mounting positions investigated by the model. Aircraft coordinates corresponding to these positions are given in Table 2.

TABLE 2. Model-calculated flow characteristics—Electra.

Location	FS	BL	WL	Y (cm)	$\frac{V_T}{V_\infty}$	α (deg)	β (deg)
A	208.0	41.2	231.2	59.0	0.993*	4.1	0.5
B	215.0	0.0	236.0	46.0	1.068	2.3	0
	215.0	0.0	236.0	46.0	1.066**	1.6	0
C	295.0	0.0	236.0	46.0	1.024	1.2	0
	295.0	0.0	236.0	46.0	1.024**	0.5	0
D	208.0	85.6	158.0	46.0	0.997*	4.4	2.4
	206.0	79.0	155.0	28.0	1.009*	4.4	2.1
	206.0	79.0	155.0	28.0	1.088	3.8	2.0
E	550.2	585.0	166.6	1313.0	1.033	7.0	−0.1
F	550.2	585.0	118.6	1313.0	0.964	4.9	+3.0
G	60.0	80.0	126.0	107.0	0.956	1.6	7.5
	60.0	68.0	126.0	76.0	0.942	1.0	9.5
H	58.0	78.0	151.0	107.0	0.949	4.0	7.8
	58.0	66.0	151.0	76.0	0.932	4.6	9.8

* With PMS canister modeled.
** 1° angle of attack.
Notes: All calculations are for 3° angle of attack except as noted. Locations are as shown in Fig. 9. Here, Y is distance out, normal to fuselage; V_T/V_∞ is ratio of flow speed at target location to freestream speed; α is the vertical flow angle with respect to longitudinal (FS) axis (positive values up); β is the horizontal flow angle with respect to longitudinal (FS) axis (positive values away from fuselage).

performed with the aircraft at a 1° (as well as the standard 3°) angle of attack for the overhead mounting locations *B* and *C*. The following discussion refers to Table 2.

For the locations modeled with the PMS probe canister (*A* and *D*), the flow speed at the sampling point is not predicted to be substantially different from freestream; this is because air that begins to accelerate around the aircraft is forced to slow again as it approaches the canister. In contrast, the flow speed is almost 9% higher than freestream without the canister at position *D*. Farther aft at position *C*, the flow speed without the canister is only 2.4% higher than freestream.

Large flow angle deviations are calculated to occur at the side-mounting location (*D*). Our results agree qualitatively with the observations of Huebert et al. (1990), who sampled aerosol particles at this location and observed that particles were deposited asymmetrically inside the sampler inlet. Removal of the PMS canister reduces the incident flow angles slightly. Angle-of-attack variations examined at positions *B* and *C* had a relatively small impact on flow velocity, with the greatest effect of reducing attack angle being to reduce the incident flow angle with respect to the fuselage. Although the impact of attack angle on droplet trajectories was not examined in this study, others have shown potentially large effects of attack angle on concentrations of some droplet sizes in regions of strong curvature (Drummond and MacPherson 1985; Norment 1988).

Locations near the aircraft nose (*G* and *H*) exhibit significant flow speed decreases and large flow angle deviations, even at distances more than 1 m from the aircraft fuselage. To investigate the flow at the wingtip locations (*E* and *F*), the wing itself was paneled. The potential flow code treats these panels as lifting elements in order to generate the proper flow behavior about the wing. The wingtip vortices are evidenced by the substantial angular distortion at locations *E* and *F*. Concentration ratios have not been calculated for the wingtip locations; the fuselage itself should have little effect on droplet distributions at these locations, although the flow field around the wingtip may influence droplet orientation and number concentration (MacPherson and Baumgardner 1988).

2) DROPLET TRAJECTORIES

Figure 10 displays calculated concentration ratios and factors as a function of droplet size for the overhead PMS location (*A*), 59 cm from the fuselage. As with the King Air (Fig. 8), the plot displays a characteristic peak at about 150 μm in diameter. Concentration ratios and factors converge for very large (1000 μm) droplets because the speed of these droplets is approximately equal to the freestream speed. The speed of a 30-μm droplet differs considerably from the freestream speed; hence, there is a noticeable difference between concentration ratio and factor. A similar situation is depicted in Fig. 11 for the overhead mounting location (*B*) in the center of the aircraft. Here, however, peak en-

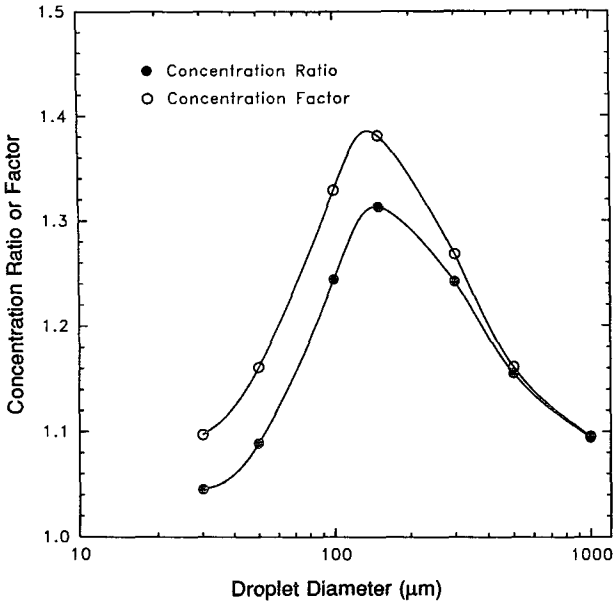

FIG. 10. Calculated concentration ratios and factors as a function of droplet diameter for Electra overhead PMS mounting location (position *A*).

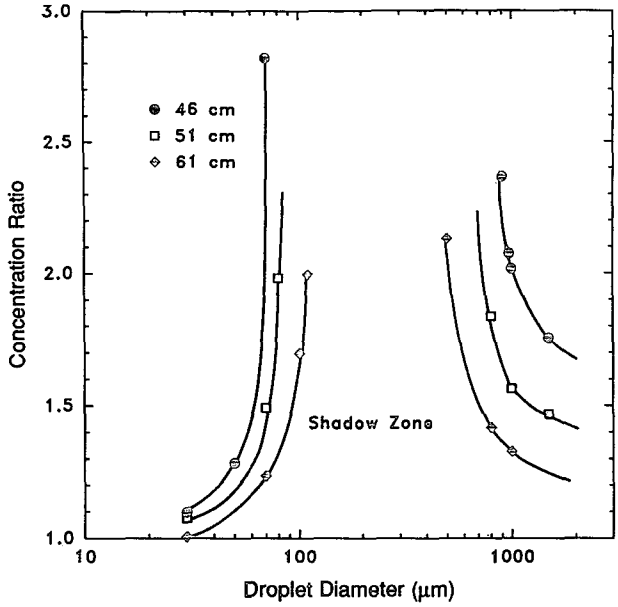

FIG. 12. Calculated concentration ratios as a function of droplet diameter at 61, 51, and 46 cm from the fuselage for second overhead location on Electra (position *C*).

hancements are much higher. This is probably because this sampling location, although approximately the same distance behind the aircraft nose, is only 46 cm from the fuselage.

Figure 12 demonstrates the effect of moving farther aft on the aircraft; location *C*, like *B*, is on the aircraft centerline, but is over 2.0 m farther back. At 46 cm from the fuselage, a shadow zone is observed for droplets approximately 80–700 μm in diameter, and other droplet sizes are predicted to experience considerable enhancement. At distances farther from the fuselage, effects are less severe, but the shadow zone persists out to 61 cm for some droplet sizes. (This does not necessarily mean that this location should be avoided for all sampling, however. Because the flow speed and angles are closer to freestream and the location is shielded from most large droplets, it may actually be more suitable for aerosol sampling than other locations!)

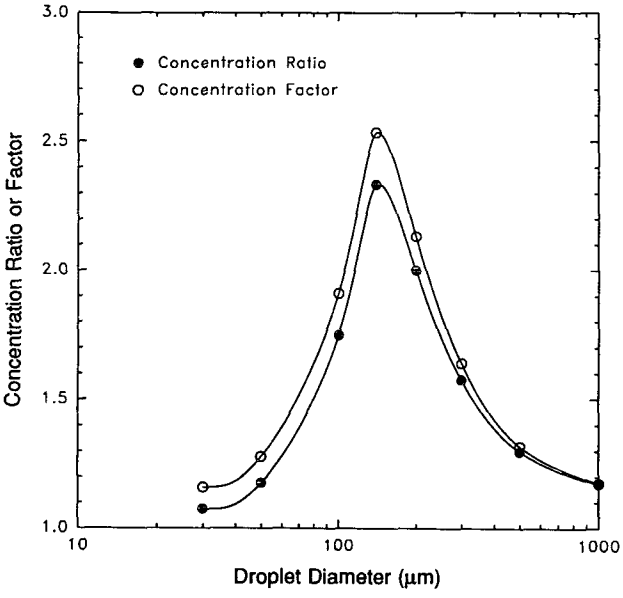

FIG. 11. Calculated concentration ratios and factors as a function of droplet diameter for Electra overhead center location (position *B*).

Finally, Fig. 13 exhibits concentration ratios for the two side-mounting configurations *D* (both modeled with the PMS canisters). At 28 cm from the fuselage, considerable enhancement of intermediate-sized droplets is evident, but at 46 cm, conditions improve markedly. Trajectories of 100-μm droplets were also calculated for the point 28 cm from the fuselage without the PMS canister. The corresponding concentration ratio was 2.26, compared with 2.39 for the same case with the canister. The flow speed was almost 9% greater than freestream without the canister, but only 1% greater with the canister. Thus, the canister apparently has a smaller effect on droplet trajectories than on flow speed at this location.

5. Summary

Flow velocities and droplet distributions present around a moving aircraft can vary substantially from freestream values, especially for locations near the fuselage and in regions of strong curvature. The effect of

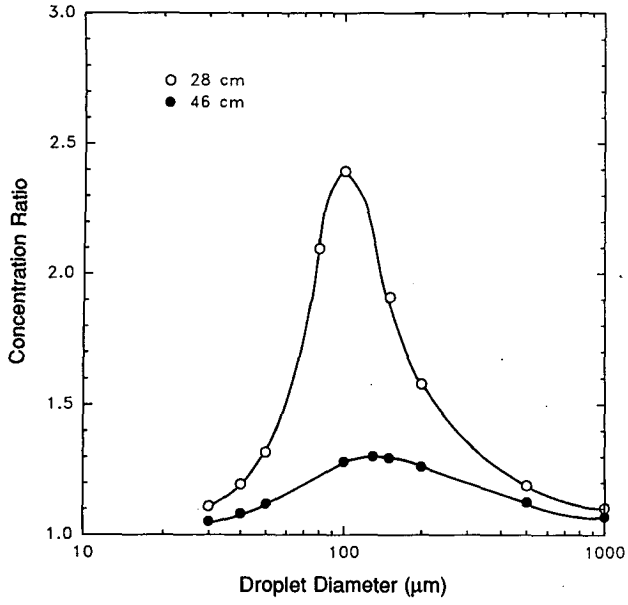

FIG. 13. Calculated concentration ratios as a function of droplet diameter at 46 and 28 cm from the fuselage for Electra side location (position *D*).

distorted streamlines on droplet trajectories is a strong function of droplet size: small droplets tend to follow flow streamlines, while large droplets deviate most from streamlines, maintaining their initial velocities and distributions. Intermediate-sized droplets undergo the greatest changes from their freestream concentrations because they partially deviate from flow streamlines.

Knowledge of the flow field can be important for the measurement of all particle and droplet sizes. For example, aerosol particle sampling may be affected by flow speed and angle changes. Cloud droplets 100–200 μm in diameter are especially likely to experience shadowing effects or enhancement of their number over ambient concentrations. Potential flow and droplet trajectory calculations, which predict these effects, are useful tools for understanding the airflow and droplet distributions around a moving aircraft.

Three overhead mounting locations on the King Air were studied in detail; our analysis showed that substantial differences in flow characteristics and droplet distributions may exist when comparing forward and aft mounting locations. Calculations predicted that flow speed was enhanced with respect to freestream values at all overhead locations, but was closer to freestream and better aligned with the aircraft fuselage at the rear locations. Droplets 145 μm in diameter were predicted to have the greatest enhancement from their freestream number concentration. Model accuracy in the rear mounting location (behind the wing) may suffer from neglect of the aircraft boundary layer and wing.

A technique for determining flow speed using a hot-wire probe was not able to verify calculated flow speeds around the King Air because of uncertainties in various parameters affecting hot-wire response (Appendix); a pitot-static system would be more suitable for flow speed measurement. Measurements with the hot-wire probe did, however, show evidence of enhancement in liquid water content at the forward mounting location between about 6 and 19 cm from the fuselage. Droplet trajectory calculations indicated that droplets 20–50 μm in diameter would be concentrated in this region. Measurements also suggested depletion of some droplet sizes near the fuselage, with depletion extending to greater distances from the fuselage in the aft mounting location.

The potential for instruments to create flow disturbances downstream was seen in the periodic variation of the retractable probe signal when the probe was mounted downstream of a CVI. A periodic variation in the aircraft sideslip angle apparently caused the retractable probe to move in and out of the turbulent wake of the CVI, with consequent changes in the flow speed derived from the retractable probe signal.

A variety of mounting locations on the NCAR Electra were studied, and all locations were calculated to experience flow distortion effects. Locations near the aircraft nose and windscreen were predicted to have the largest departures of flow angle and speed from freestream. At aft locations, flow characteristics were closer to freestream, but deleterious effects on droplet distributions were more pronounced. A shadow zone was predicted for one aft location, and it persisted for some droplet sizes out to 61 cm from the fuselage. PMS canisters were shown to have a large effect on local flow speed (as discussed by others), but little influence on droplet concentrations at sampling points ahead of the canisters. Reducing the aircraft angle of attack had the effect of reducing the incident flow angle slightly.

The comparison of these calculation results with measurements revealed some of the potential sources of error in both, and more measurements to verify the calculations would certainly be useful. Predictions from the model seem reliable for locations ahead of the aircraft wing; we therefore feel that the information it provides for these locations is preferable to the rough guidelines that are sometimes used. It is hoped that the many mounting locations and conditions that have been simulated here will lead to more optimal placement of instrumentation on the aircraft in the future.

Acknowledgments. Special thanks to the referenced investigators who provided foundation for this work and to the NCAR Visiting Scientist and Advanced Studies Program for financial support of the authors. Hillyer Norment furnished the potential flow and droplet trajectory codes and constructed the paneled models of the aircraft fuselages. From RAF, we wish to thank Norm Zrubek for designing the retractable strut, Paul LeHardy for installing and operating the probes, the pilots of the King Air, and Barbara Knowles for administrative assistance. Thanks are also due to

Greg Kok for suggesting the experimental technique and to Darrel Baumgardner for aid in the data analysis and for several useful suggestions.

APPENDIX

Calculation of Flow Speed from PMS–CSIRO Hot-Wire Probe

As discussed in the text, flow speed as well as liquid water content was expected to vary with distance from the fuselage. The assumption that flow speed was constant led to large excursions from zero of the baseline signal of the retractable hot-wire probe at different distances from the fuselage. A method to estimate the change in flow speed with distance from the fuselage is presented here, using the response of the probe in the fully extended position (43 cm from the fuselage) as a reference.

The amount of power P_d required to maintain the probe sensor at a constant temperature in dry air is related to the wire temperature T_w, air temperature T_a, sensor length l, thermal conductivity k, and the Nusselt number Nu, as follows:

$$P_d = \pi lk(T_w - T_a)\,\mathrm{Nu}.$$

The Nusselt number can be parameterized in terms of the Reynolds number Re and the Prandtl number Pr (where Pr is defined as the specific heat of air at constant pressure times viscosity divided by thermal conductivity):

$$\mathrm{Nu} = A\,\mathrm{Re}^x\,\mathrm{Pr}_f^y\left(\frac{\mathrm{Pr}_f}{\mathrm{Pr}_w}\right)^z.$$

Subscripts f and w represent the film temperature and the wire temperature of the probe element. In our analysis, the film temperature (temperature at the interface between the wire and ambient air) was estimated to be the average of the wire and ambient temperatures. Ambient temperature was initially assumed to equal the corrected temperature derived from a Rosemount type 102 sensor on the aircraft nose. The values of the coefficient A and exponents x, y, and z vary slightly with Reynolds number, but can be considered constant under our flight conditions and were given the empirically derived values of 0.26, 0.60, 0.37, and 0.25, respectively, for $10^3 < \mathrm{Re} < 2 \times 10^5$ (Zukauskas and Ziugzda 1985). Turbulence can also cause cooling of the heated wire, and this treatment assumes a freestream turbulence level of about 1%. If the dry air power loss is measured, the Nusselt number, Reynolds number, and ultimately the local flow speed can be calculated, since

$$\mathrm{Re} = \frac{\rho V d}{\eta},$$

where ρ is the air density, V the flow speed, d the sensor diameter, and η the air viscosity.

Flow speed is required to calculate liquid water content from the hot-wire probe as described in section 3b, but the determination of speed as described above is only possible in clear air. A linear relationship between the probe flow speed and the radome-measured airspeed was therefore determined empirically for each distance from the fuselage used on each flight; this relationship was then used to calculate the probe flow speed and liquid water content in cloud.

One difficulty with this technique is that the probe wire and film temperatures are needed to calculate flow speed, but these temperatures are not precisely known, as they vary from probe to probe. Therefore, a wire temperature that generated the smallest average power offset and variance throughout the clear-air regions of each flight was calculated for each probe at 43 cm from the fuselage; this wire temperature was assumed to remain constant with distance from the fuselage. To perform this calculation, a flow speed value was required, for which the aircraft true airspeed (measured by the differential pressure system in the radome) was used as an initial estimate. Unfortunately, this caused the calculated speed at $Y = 43$ cm to be approximately equal to the radome-measured airspeed; model results suggest that flow speeds at these locations are actually greater than the aircraft speed by about 5% and 2% at FS 155 and 263, respectively. The *absolute* liquid water contents calculated here will therefore be in error by the ratio of flow speed at the radome to that at 43 cm, but the *relative* change in liquid water content at various distances from the fuselage should not be biased by this process.

It was initially assumed that the ambient air density and temperature were constant with distance from the fuselage. The constant-temperature assumption is a potential source of error, since pressure and temperature will actually vary with flow speed, and speed results from the hot-wire probe are dependent on air temperature. An increase in flow speed should cause a decrease in pressure and, assuming constant density, temperature at the hot-wire location. However, a decrease in the assumed probe temperature would result in a decrease in flow speed calculated by this technique. Iterative methods were used to calculate a relative speed and air temperature at each distance that was consistent with both the constant-density assumption and the preceding equations. Using this approach, we found that the constant-temperature simplification caused speed changes calculated from the hot-wire probe to be slightly overestimated; for example, the maximum speed increase measured between 43 and 21.5 cm at FS 263 was about 7% with the constant-temperature assumption and about 5.5% without it. Although the liquid water contents presented in the text were obtained using the invariant temperature, the potential errors of this approach are less than about 2% and are incorporated into the error bars in Figs. 2 and 3.

The speeds determined from both probes by the

foregoing method agreed to within about 1 m s^{-1} (1%) at the fully extended position. When the fixed probe was used as a flow speed reference for comparison to the retractable probe measurements at various distances from the fuselage, large differences were found in flow speed profiles between the rear and forward locations.

Flow speed data at 4–43 cm from the fuselage in the forward position exhibited considerable scatter, although the maximum change in speed relative to that at 43 cm was 2.2%. We found that the calculated speed was very sensitive to the wire temperature used; a 1° difference in wire temperature resulted in about a 1% difference in calculated flow speed. For the particular flight during which these data were obtained, the wire temperature, or possibly the film temperature derived from it, apparently drifted substantially with time (the wire temperature that produced the smallest zero offset out of cloud varied by up to 4°). Freestream turbulence levels greater than 1% are not considered in this treatment and can substantially influence heat transfer from the wire; the precise impact of turbulence is dependent on the length scale of the turbulence as well as its intensity. These uncertainties could cause the flow speed determined from the hot-wire to be in error by up to a few percent. Airflow calculations predicted only a 1% increase in speed between 43 and 13 cm. Therefore, we consider the measurements in this location inadequate to determine the actual speed variation with distance from the fuselage.

When the probe was mounted in the rear location, the wire temperature seemed to be stable, but the speed changes determined from the hot-wire probe were much larger than those predicted by the airflow calculations. The measurements indicated a speed increase of about 5.5% between 43 and 21.5 cm and a steady decrease in speed below 21.5 cm to about 4.5% less than the reference speed at 4 cm from the fuselage. The decrease in speed at distances very near the fuselage (in the boundary layer) cannot be simulated by potential flow calculations; however, these calculations predicted less than a half percent increase in speed between 43 and 21 cm. As discussed in the text, the counterflow virtual impactor mounted ahead of the hot-wire in the rear location apparently produced a turbulent wake that was not considered by either the airflow calculations or the hot-wire analysis. This and the lack of the wing and boundary layer in the airflow model probably explains the discrepancies between the measurements and simulations.

The hot-wire probe is less than ideal for measuring flow speed because of the assumptions that must be made. In the future, measurements using a pitot-static system should provide more accurate speed results for comparison with the model.

REFERENCES

Beard, K. V., 1983: Reorientation of hydrometeors in aircraft accelerated flow. *J. Chem. Appl. Meteor.*, **22,** 1961–1963.

Cooper, W. A., and D. Rogers, 1991: Effects of airflow trajectories around aircraft on measurements of scalar fluxes. *J. Atmos. Oceanic. Technol.*, **8,** 66–77.

Drummond, A. M., and J. I. MacPherson, 1985: Aircraft flow effects on cloud drop images and concentrations measured by the NAE Twin Otter. *J. Atmos. Oceanic Technol.*, **2,** 633–643.

Huebert, B. J., G. L. Lee, and W. L. Warren, 1990: Airborne aerosol inlet passing efficiency measurement. *J. Geophys. Res.*, **95,** 16 369–16 381.

King, W. D., 1984: Air flow and particle trajectories around aircraft fuselages. I: Theory. *J. Atmos. Oceanic Technol.*, **1,** 5–13.

——, 1985: Air flow and particle trajectories around aircraft fuselages. III: Extensions to particles of arbitrary shape. *J. Atmos. Oceanic Technol.*, **2,** 539–547.

——, 1986: Air flow and particle trajectories around aircraft fuselages. IV: Orientation of ice crystals. *J. Atmos. Oceanic Technol.*, **3,** 433–439.

——, D. A. Parkin, and R. J. Handsworth, 1978: A hot-wire probe having fully calculable response characteristics. *J. Appl. Meteor.*, **17,** 1809–1813.

——, C. T. Maher, and G. A. Hepburn, 1981: Further performance tests on the CSIRO hot-wire probe. *J. Appl. Meteor.*, **20,** 195–202.

——, D. E. Turvey, D. Williams, and D. J. Llewellyn, 1984: Air flow and particle trajectories around aircraft fuselages. II: Measurements. *J. Atmos. Oceanic Technol.*, **1,** 14–21.

Knollenberg, R. G., 1981: Techniques for probing cloud microstructure. *Clouds: Their Formation, Optical Properties and Effects,* P. V. Hobbs and A. Deepak, Eds., Academic Press, 494 pp.

MacPherson, J. I., and D. Baumgardner, 1988: Airflow about King Air wingtip-mounted cloud particle measurement probes. *J. Atmos. Oceanic Technol.*, **5,** 259–273.

Norment, H. G., 1976: Effects of airplane flow fields on hydrometeor concentrations. *Preprints, Int. Conf. on Cloud Physics,* Amer. Meteor. Soc., Boulder, 591–596.

——, 1985: Calculation of water drop trajectories to and about arbitrary three-dimensional lifting and non-lifting bodies in potential airflow. NASA Contractor Report 3935, National Aeronautics and Space Administration, 166 pp. [NTIS N87-11694/3/GAR.]

——, 1988: Three-dimensional trajectory analysis of two drop sizing instruments: PMS OAP and PMS FSSP. *J. Atmos. Oceanic Technol.*, **5,** 743–756.

Wyngaard, J. C., L. Rockwell, and C. A. Friehe, 1985: Errors in the measurement of turbulence upstream of an axisymmetric body. *J. Atmos. Oceanic Technol.*, **2,** 605–614.

Zukauskas, A., and J. Ziugzda, 1985: *Heat Transfer of a Cylinder in a Crossflow.* Hemisphere Publishing Company, 208 pp.